

United States Department of Agriculture



Natural Resources Conservation Service
National Soil Survey Center
Federal Building, Room 152
100 Centennial Mall North
Lincoln, NE 68508-3866

Phone: (402) 437-5499
FAX: (402) 437-5366

SUBJECT: MGT – Trip Report – Geophysical Field Assistance

July 20, 2012

TO: Denise Colman
State Conservationist
NRCS, Harrisburg, Pennsylvania

File Code: 330-20-7

Dr. Henry Lin
Professor of Hydropedology/Soil Hydrology
Dept. of Ecosystem Science & Management
415 Agricultural Sciences & Industries Building
Pennsylvania State University
University Park, Pennsylvania 16802

Purpose:

At the request of Dr. Henry Lin, Professor of Hydropedology, geophysical field assistance was provided by the National Soil Survey Center to the Department of Ecosystem Science and Management at Pennsylvania State University (PSU). No Pennsylvania NRCS assistance was required.

Geophysical investigations were conducted within the Shale Hills *Critical Zone Observatory (CZO)* in Huntingdon County, and at Pennsylvania State University's *Living Filter Field* in Centre County, Pennsylvania. The principal goal of the Shale Hills CZO and the associated interdisciplinary research was to quantitatively predict the creation, evolution, and structure of regolith as a function of the biologic, geochemical, geomorphologic, hydrologic and pedologic processes operating in a temperate, forested landscape. The Shale Hills CZO serves as an experimental catchment for the study of spatial and temporal variations in hydrological response. The focus of the present research is to use time-lapsed ground-penetrating radar (GPR) to identify preferential flow pathways and patterns across three water-infiltration test sites located on different soil-landscape components within the catchment. Results of GPR surveys were supported by measurements of soil moisture using multiple arrays of time-domain reflectometry probes.

In addition, the sensitivity and response functions of three electromagnetic induction (EMI) sensors (Dualem-2, EM38-MK2, and Profler) were evaluated at Pennsylvania State University's *Living Filter Field*. These three EMI sensors are used by USDA and comparative surveys are needed to document their resolution, exploration depths, and response times.

Participants:

Jim Doolittle, Research Soil Scientist, USDA-NRCS, National Soil Survey Center, Newtown Square, PA
Li Guo, Ph.D. Student, Dept. of Ecosystem Science & Management, Pennsylvania State University,
University Park, PA

Isaac Hopkins, MS Student, Dept. of Ecosystem Science & Management, Pennsylvania State University,
University Park, PA

Liu Hu, Post-Doctorate, Dept. of Ecosystem Science & Management, Pennsylvania State University,
University Park, PA

Helping People Help the Land

An Equal Opportunity Provider and Employer



Henry Lin, Professor of Hydropedology/Soil Hydrology, Dept. of Ecosystem Science & Management,
Pennsylvania State University, Philadelphia, PA

Jonathan Nyquist, Chairperson and Professor, Earth & Environmental Science, Temple University,
Philadelphia, PA

Rick Taylor, President, Dualem, Milton, Ontario, CANADA

Activities:

Field activities were completed during the period of June 12-15, 2012.

Summary:

1. Comparative GPR surveys showed that, at the time of this study, the 900 MHz antenna provided superior resolution of subsurface interfaces than the 400 MHz antenna. Both antennas provided satisfactory exploration depths for the infiltration studies.
2. Multiple, detailed, time-lapsed ground-penetrating radar (GPR) grid surveys of two *infiltration grid site* located in areas of Rushtown and Weikert soils were completed using a 900 MHz antenna. A total of 18 separate time-lapsed GPR grid surveys were completed. Each GPR survey consisted of either eight (Rushtown site) or nine (Weikert site) separate radar traverses and records (total of 168 radar records). To measure changes in soil moisture, Decagon 5TE soil moisture sensors were inserted in trenches located immediately down slope of the grid areas.
3. A detailed GPR grid survey was also completed across a *permanent grid site* using a 400 MHz antenna. This survey consisted of 12 separate radar traverses. This grid site was located in an area of Rushtown soils.
4. At the Rushtown infiltration grid site, after wetting, a cluster of noticeably higher amplitude subsurface reflections and hyperbolas appear in the central portion of 2D radar records from Line one. The presence and increased amplitudes of these reflections were attributed to increased soil water contents.
5. At the Weikert infiltration grid site, after wetting, the reflections from the soil/bedrock interface increased in amplitude. However, spatial variations in amplitudes were observed along this interface suggesting non-uniform distribution of soil moisture.
6. Two-dimensional radar records appear to provide greater immediate information on the movement of water than the time-lapsed, three-dimensional, time-sliced pseudo-images. On depth slices images, it was difficult to perceive substantial, sustained, and systematic changes in the reflective patterns that could be attributed to water flow and increased soil moisture contents. Additional, more comprehensive analysis of the 3D images should provide improved interpretations. The use of other image-analysis techniques that can quantify signal amplitudes would improve assessments of soil moisture flow.
7. At the Living Filter Field, EC_a data collected with three EMI sensors were similar. In general, slightly lower and more variable EC_a measurements were recorded with the Dualem-2 meter. Slightly higher and less variable EC_a were recorded with the EM38-MK2 meter. These small variations reflect differences in the depth of exploration and volume of soil material measured with each sensor, operating frequencies, sensor calibrations, number of recorded measurements, and soil's conductivity profiles. With minor exceptions and regardless of device, dipole geometry, frequency or exploration depth, the resulting spatial patterns appear remarkably similar.

8. Files of the radar records that were collected over the grid sites have been mailed to Dr. Henry Lin for further analysis by his students. The collected data are important to research on the infiltration of water in soils underlain by highly fractured shale.



JONATHAN W. HEMPEL
Director
National Soil Survey Center

Attachment (Technical Report)

cc:

Robert R. Dobos, Soil Scientist (NSSC Liaison for MO-13), Soil Survey Interpretations, NSSC, MS 36,
NRCS, Lincoln, NE

James A. Doolittle, Research Soil Scientist, Soil Survey Research & Laboratory, NSSC, NRCS, Newtown
Square, PA

David Kingsbury, State Soil Scientist/MLRA Office Leader, NRCS, Morgantown, WV

William R. Knight, Acting State Soil Scientist, NRCS, Harrisburg, PA

John W. Tuttle, Soil Scientist, Soil Survey Research & Laboratory, NSSC, NRCS, Wilkesboro, NC

Larry T. West, National Leader, Soil Survey Research & Laboratory, NSSC, MS 41, NRCS, Lincoln, NE

Linda A. Kruger, Secretary, Soil Survey Research & Laboratory, NSSC, MS 41, NRCS, Lincoln, NE

Technical Report on Geophysical Investigations conducted at the Shale Hills *Critical Zone Observatory (CZO)* in Huntington County and at Pennsylvania State University's Living Filter Field in Centre County on June 12-15, 2012.

James A. Doolittle

Equipment:

The radar unit is the TerraSIRch Subsurface Interface Radar (SIR) System-3000 (SIR-3000), manufactured by Geophysical Survey Systems, Inc. (GSSI; Salem, NH).¹ The SIR-3000 consists of a digital control unit (DC-3000) with keypad, SVGA video screen, and connector panel. A 10.8-volt lithium-ion rechargeable battery powers the system. The SIR-3000 weighs about 9 lbs (4.1 kg) and is backpack portable. With an antenna, the SIR-3000 typically requires two people to operate. Daniels (2004) and Jol (2008) discuss the use and operation of GPR. The 400 and 900 MHz antennas were used in this investigation.

The RADAN for Windows (version 6.6) software program (GSSI) was used to process the radar records.¹ Basic processing steps that were applied to all radar records include: header editing, setting the initial pulse to time zero, color table and transformation selection, and distance normalization. After initial processing, each set of radar records were combined into a 3D radar file, which was stacked, horizontal filtered, and migrated. Stacking is used to remove high frequency noise that appears *snow-like* on radar records. A horizontal high pass (background removal) filter is used to remove horizontal bands of lower frequency (wider band widths) noise that obscured real reflections. Migration is used to reduce noise associated with hyperbolic diffraction patterns and more properly align inclined interfaces. In addition, data were transformed using a Hilbert transformation envelope. Hilbert transformation uses the magnitude of the return signal to decompose multiple hyperbolic reflections into more compact and representative forms (Daniels 2004).

Calibration of GPR:

Ground-penetrating radar is a time scaled system. The system measures the time that it takes electromagnetic energy to travel from an antenna to an interface (e.g., bedrock, soil horizon, stratigraphic layer) and back. To convert the travel time into a depth scale, either the velocity of pulse propagation or the depth to a reflector must be known. The relationships among depth (D), two-way pulse travel time (T), and velocity of propagation (v) are described in equation [1] (after Daniels, 2004):

$$v = 2D/T \quad [1]$$

The velocity of propagation is principally affected by the relative dielectric permittivity (E_r) of the profiled material(s) according to equation [2] (after Daniels, 2004):

$$E_r = (C/v)^2 \quad [2]$$

Where C is the velocity of propagation in a vacuum (0.3 m/ns). Typically, velocity is expressed in meters per nanosecond (ns). In soils, the amount and physical state (temperature dependent) of water have the greatest effect on the E_r and v. At the time of these studies, soils were moist.

¹ Manufacturer's names are provided for specific information; use does not constitute endorsement.

Based on the measured depth and the two-way pulse travel time to a known subsurface reflector (metal plate buried at 50 cm), the velocity of propagation and the relative dielectric permittivity through the upper part of soil profiles were estimated using equations [1] and [2]. The calibration site was located in an area of Rushtown soils. For the 400 MHz antenna, an estimated v of 0.0917 m/ns resulted in an E_r of 10.7. For the 900 MHz antenna, an estimated v of 0.0810 m/ns resulted in an E_r of 13.72. It must be noted that using one E_r value for transforming travel times into depth scales generally lead to slightly distorted values due to assumption of uniform layers with constant E_r and not accounting for spatial and depth variations in the soil architecture and moisture contents.

Field Methods:

Permanent Grid Site:

The permanent grid was located on the lower portion of a swale that was dominated by Rushtown soils. The very deep, excessively drained Rushtown soils formed in colluvial deposits. Rushtown is a member of the loamy-skeletal over fragmental, mixed, active, mesic Typic Dystrudepts family.

Twelve parallel, 15-ft (4.57 m) long traverse lines spaced at intervals of about 13-inch (33 cm) form a 15 by 12 ft (4.57 by 3.66 m) grid. The X-axis of this grid was orthogonal to the long axis of the swale. Plastic stakes have been inserted in the ground at the four grid corners. A rope grid-lattice was attached to the four plastic stakes and overlays the grid area. The rope lines provide a grid lattice and ground control. Each rope line was distance-graduated with marks at 5 ft (1.524 m) intervals for ground-control.

A GPR survey was conducted by pulling the 400 MHz antenna along each of the traverse lines from west to east (one-way). Following data collection along a traverse line, the antenna was sequentially moved about 13 inches along the Y axis to the next rope line, and the process was repeated. A total of 12 traverses were required to complete the GPR survey of the permanent grid site.

Infiltration Grids:

Repetitive GPR surveys were conducted across two small grids to observe temporal changes in subsurface reflections associated with changes in soil moisture caused by artificially introduced water flow using a line source. The grids were located on different soil/landscape components. Traverse lines were orientated essentially orthogonal to the slope. The distance between successive traverse lines was 10 cm. Repeated GPR surveys were conducted with a 900 MHz antenna along the traverse lines prior to infiltration and at various times after the infiltration (e.g., 0, 15, 30, 45, 60 and 120 min). Three-dimensional (3D) pseudo-images of the infiltration grid sites were prepared from each set of radar records. These sets of radar records were subjected to the same processing procedures.

Rushtown Grid:

This infiltration grid site was located in a swale dominated by Rushtown soils. The dimensions of the Rushtown infiltration grid were 210 by 70 cm. Each survey consisted of 8 parallel GPR traverses, which were conducted from west to east across the grid site. Each traverse was 210-cm long. Distance graduated ropes were used to guide the antenna. These ropes were spaced at 10-cm intervals across the grid site. Marks were affixed to the distance graduated rope at intervals of 30 cm and served as ground control.

A line source of water infiltration (a 1-m long, 10-cm deep trench) was located immediately upslope of the grid. Decagon 5TE sensors (Pullman, Washington) were installed in a trench located immediately down-slope of the grid.² These sensors were inserted into the upslope sidewall of the trench. These sensors are designed to measure soil moisture, soil temperature, and bulk electrical conductivity (EC).

² Manufacturer's names are provided for specific information; use does not constitute endorsement.

Weikert Grid:

This infiltration grid site was located on a plane, upper side-slope dominated by Weikert soils. The shallow, well drained Weikert soils formed in material weathered from interbedded acid shales. Weikert is a member of the loamy-skeletal mixed, active, mesic Lithic Dystrudepts family.

The dimensions of the Weikert infiltration grid were 300 by 80 cm. To complete a GPR survey, nine, 300-cm long traverses were completed across the grid with a 900 MHz antenna. The traverses were conducted from west to east across the grid site. Distance graduated ropes were used to guide the antenna. These ropes were spaced at 10-cm intervals across the grid site. Marks were affixed to the distance graduated rope at intervals of 50 cm and served as ground control. A line source of water infiltration (a 1-m long, 10-cm deep trench) was located immediately upslope of the grid. Decagon 5TE sensors were installed in a trench located immediately down slope of the grid.

Results:

Permanent Grid:

Figure 1 is a 3D-GPR pseudo-image of the permanent grid site. This pseudo-image was prepared from data collected with a 400 MHz antenna. In Figure 1, a 2 x 3 x 1 meter inset cube has been graphically removed from the pseudo-image. The base of this inset cube rests on a dense subsurface layer, which provides higher amplitude (colored white and black) reflections.

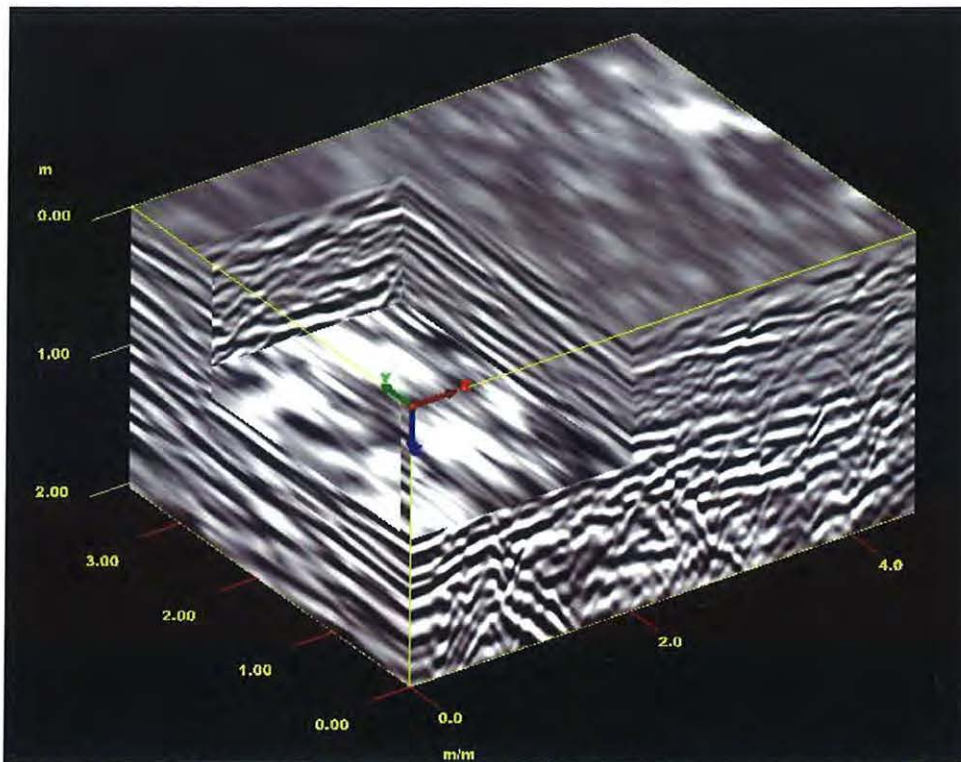


Figure 1 - This 3D pseudo-image of the permanent grid site was constructed from twelve radar records that were collected with a 400 MHz antenna.

In the 3D pseudo-image shown in Figure 1, a sequence of stratigraphic layers was evident within the column of colluvium that fills the swale. This 3D pseudo-image provides a means of visualizing and interpreting the 3D continuity of the different layers. Strata vary in grain-size distribution, rock fragments, moisture, and/or density. The higher the amplitude of the reflected signals the more abrupt and contrasting the difference in dielectric properties across the interface. As radar scans are

continuously collected in the direction of the radar traverse (along the X axis; right foreground), subsurface features are better resolved along the direction of radar travel. In the orthogonal direction to the radar traverse (along the Y axis), images are interpolated between successive GPR traverses (spaced at 33 cm intervals). These images are, therefore, more poorly resolved and appear smudged.

In the 3D pseudo-image shown in Figure 1, migration was used to reduce noise associated with hyperbolic diffraction patterns and more properly align inclined interfaces. However, a large number of hyperbolas and diffraction tails persist in this 3D pseudo-image. Previous GPR work within the catchment has associated the scattering of radar reflections to inhomogeneities in the soil and the non-uniform distribution of water.

GPR Survey of Infiltration Grid:

Repetitive GPR surveys were conducted across the two small *infiltration grid sites* to observe temporal differences in subsurface reflections associated with the flow of water through profiles of Rushtown and Weikert soils. Appendix 1 lists the radar file numbers associated with different traverses within these sites.

Rushtown Infiltration Grid Site:

Comparative GPR surveys were conducted with the 400 and 900 MHz antenna. As a general rule, the higher the center frequency of an antenna, the greater the resolution of subsurface features. However, higher frequency antennas suffer greater attenuation rates resulting in more restricted exploration depths. Figure 2 and 3 are 3D-GPR pseudo-images of the Rushtown site. The pseudo-image in Figure 2 was prepared from data collected with the 400 MHz antenna. The pseudo-image in Figure 3 was prepared from data collected with the 900 MHz antenna. In each pseudo-image, a 1 x 40 x 60 cm inset cube has been removed to provide additional stratigraphic details.

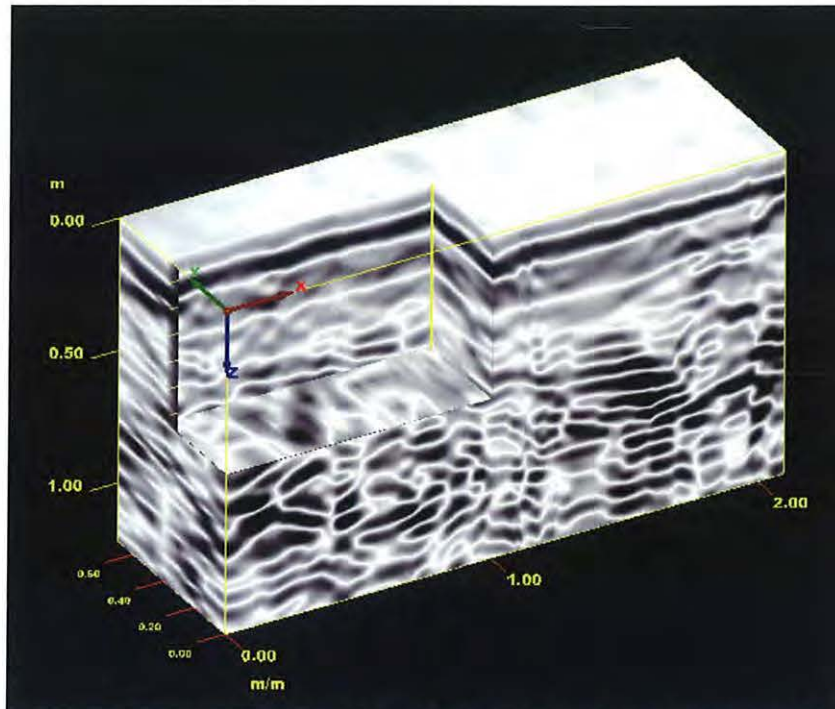


Figure 2 - This 3D pseudo-image of the Rushtown Infiltration site was prepared from data collected with a 400 MHz antenna. A 100 x 40 x 60 cm inset cube has been removed from the pseudo-image.

In the 3D pseudo-images shown in Figure 2 and 3, inclined reflection patterns were evident. These

reflectors, which vary in amplitude and expression, represent different strata within the colluvium. Strata vary in grain-size distribution, rock fragments, moisture, and/or density. As evident in these 3D pseudo-images, these strata appear laterally discontinuous with noticeable breaks in their continuity. These breaks were associated with potential preferential flow pathways. Comparing Figures 2 and 3, it is evident that the 900 MHz antenna provides superior resolution of subsurface features and as satisfactory an exploration depth as the 400 MHz. This was at first surprising, as the soils have a clay content of 28 to 32 % in the upper soil layers. It was assumed that this material would be too attenuating to the 900 MHz antenna. This was not the case. It was decided to use the 900 MHz antenna for the time-lapsed infiltration studies conducted at the Rushtown and Weikert sites.

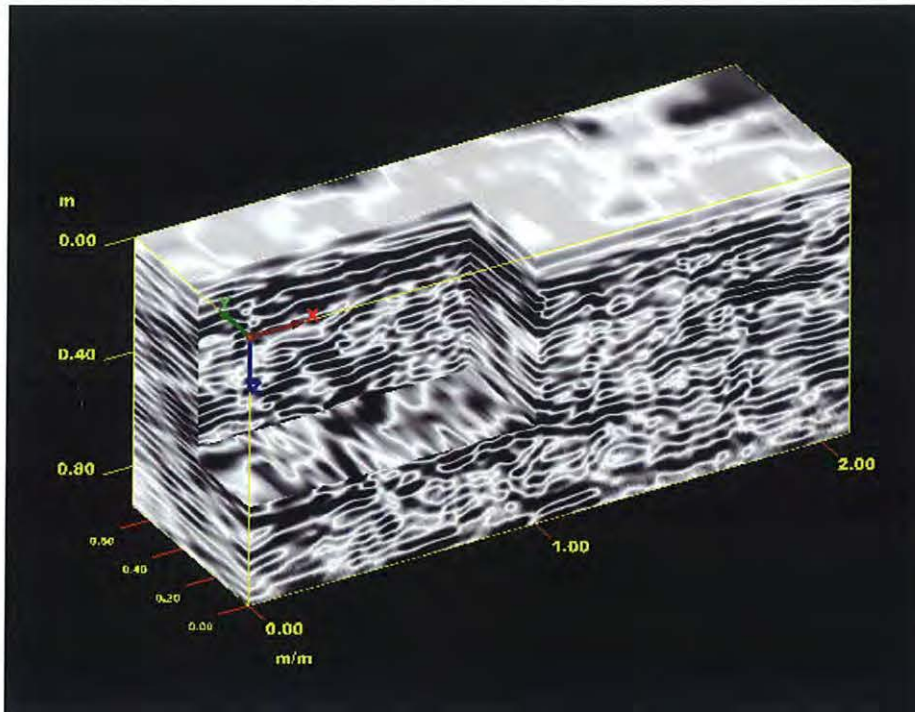


Figure 3 - This 3D pseudo-image of the Rushtown Infiltration Grid Site was prepared from data collected with a 900 MHz antenna. A 100 x 40 x 60 cm inset cube has been removed from the pseudo-image.

Figure 4 contains six, time-lapsed 2D radar records from Line 1 of the Rushtown infiltration grid site. This line was closest to the infiltration trench and, therefore, should be the first line affected by the flow of infiltrating water. A cluster of noticeably higher amplitude reflections and hyperbolas appear in the central portion of the radar records 15 to 60 minutes after wetting. The emergence and increased amplitudes of these reflections were attributed to increased water contents. Some variations in reflective patterns and amplitudes on these radar records are caused by variations in the placement of the radar traverse, and antenna alignment and jarring.

In Figure 5, six different, time-lapsed, radar records from Line 1 of the Rushtown Grid have been transformed using a Hilbert transformation envelope. Apparent on these transformed 2D radar records is the development and vertical extension of high magnitude reflections in the central portion of this line after the infiltration experiment was begun. Between depths of about 50 and 75 cm, noticeable bands of high magnitude reflections were evident in the central portion of this line. These higher magnitude reflections may represent the accumulation and partial infiltration of water through a denser subsurface layer. The development of these high magnitude reflections is attributed to increased soil moisture. If

this interpretation is correct, these patterns suggest that moisture moves fairly rapidly downward and laterally through Rushtown soils.

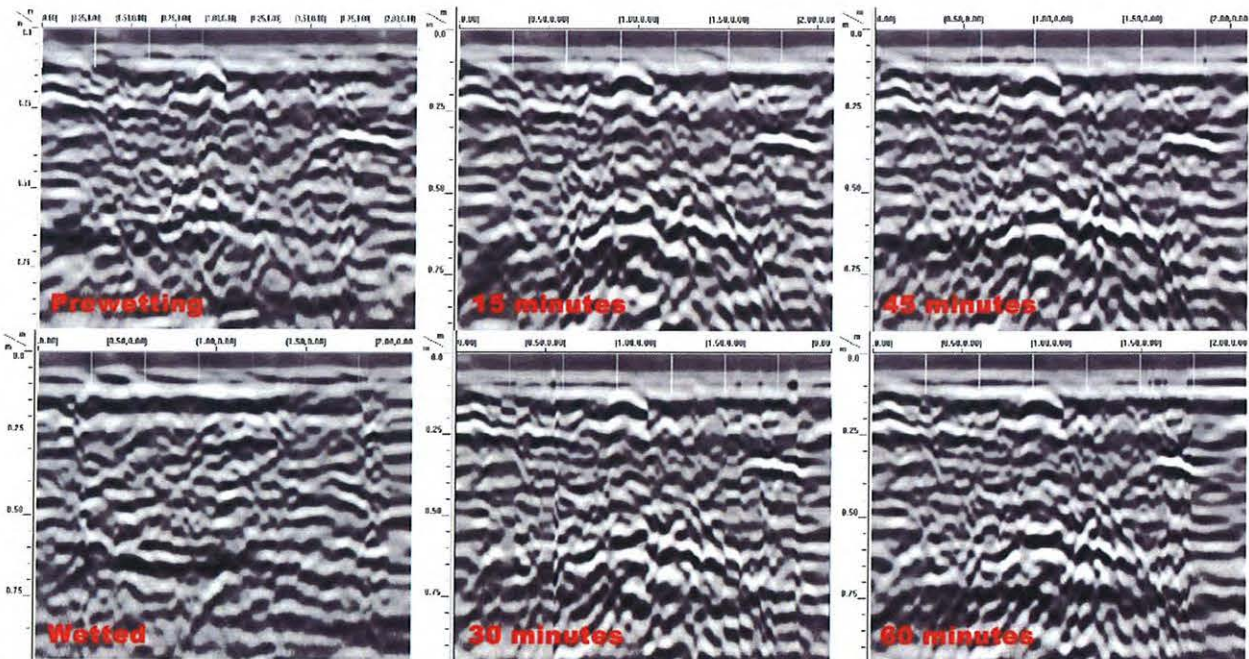


Figure 4 - Time-lapsed 2D radar records of Line 1 at the Rushtown Infiltration Grid Site. All scales are in meters.

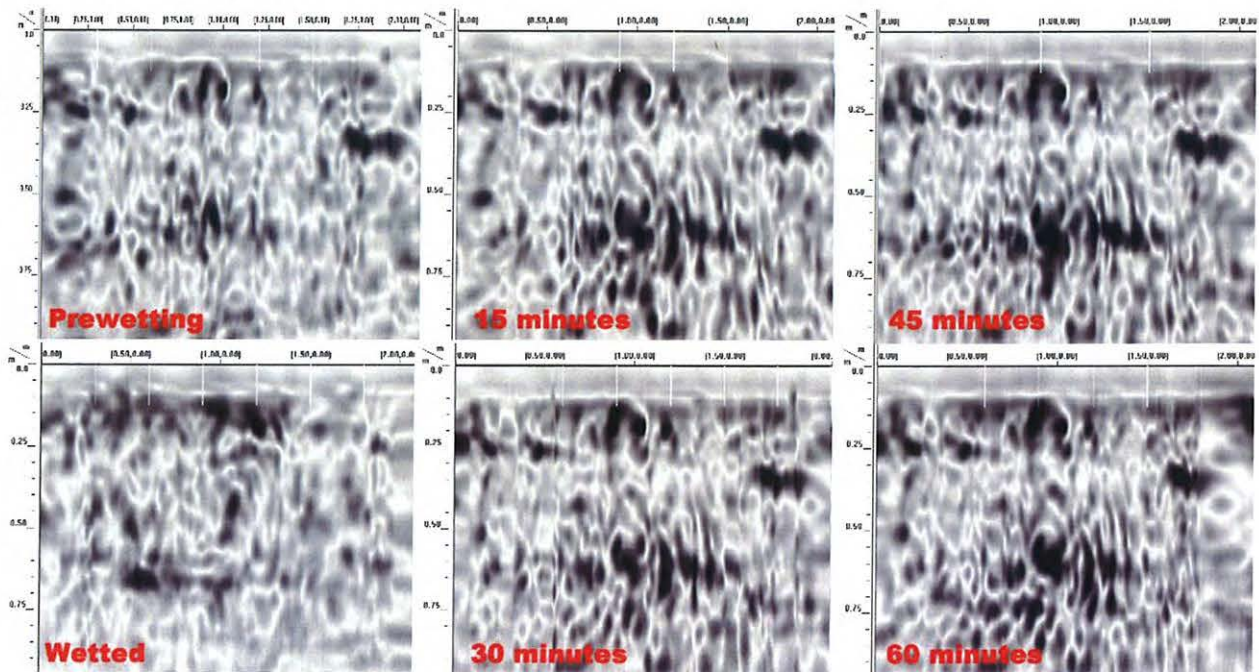


Figure 5 - Time-lapsed Hilbert Transformed 2D radar records from Line 1 at the Rushtown Infiltration Grid Site. All scales are in meters.

Figure 6 contains six Hilbert transformed, time-lapsed, depth-sliced pseudo-images for the 30 and 60 cm

depth intervals. The time intervals span the duration from “pre-wetting” to 60 minutes following infiltration. The thickness of each slice was 10 cm. Variations in signal amplitudes and spatial patterns were evident in these plots. However, in the depth slices shown in Figure 6, it is difficult to perceive systematic changes in the reflective patterns that can be attributed to water flow and increased soil moisture contents.

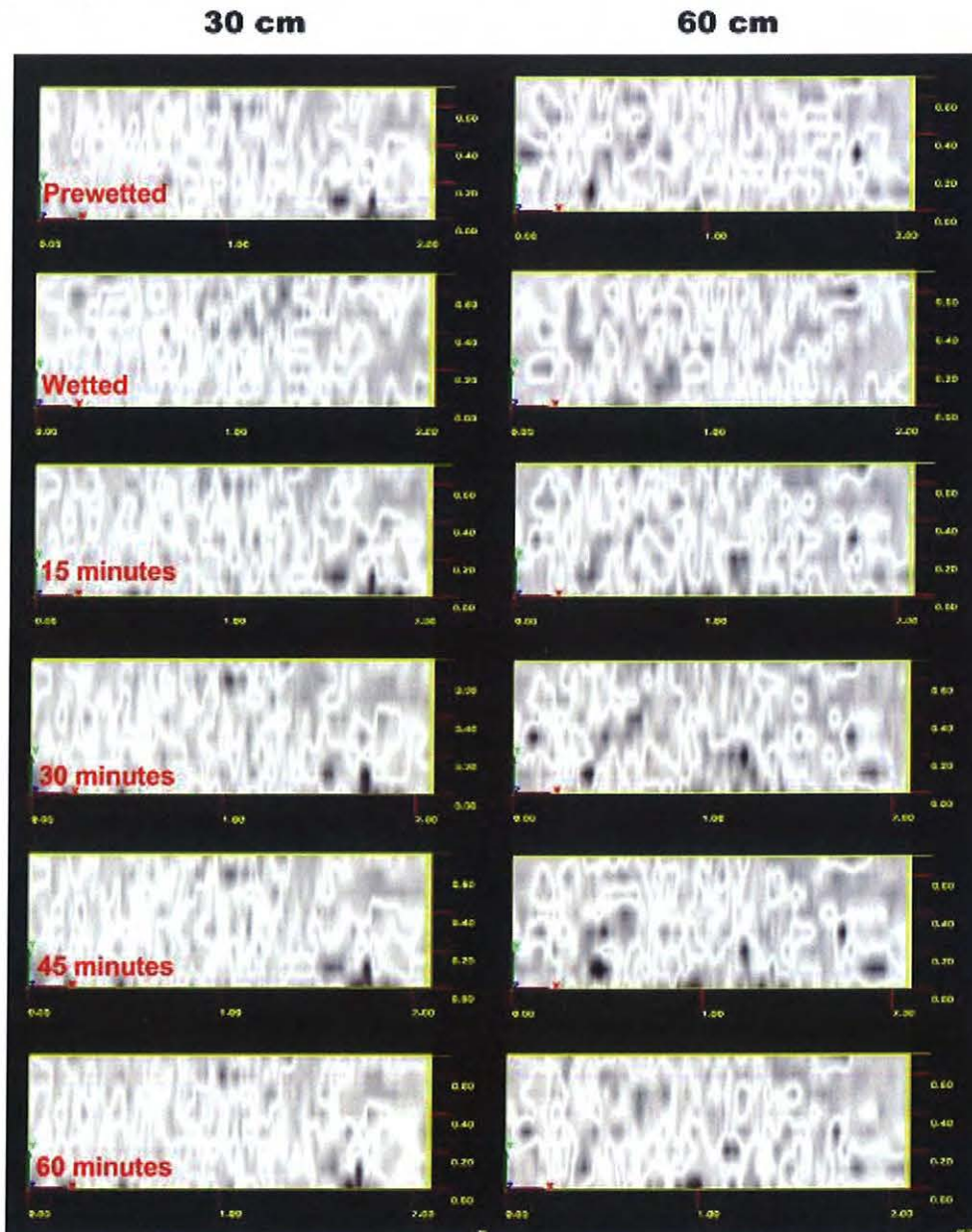


Figure 6 - These time-lapsed, depth-sliced pseudo-images from the Rushtown Infiltration Site are for the 30 (left) and 60 (right) cm depth intervals. View is looking down on the grid from directly overhead.

Weikert Infiltration Grid Site:

Figure 7 is a three-dimensional (3D) GPR pseudo-image of the Weikert infiltration grid site. This pseudo-image was prepared from data collected with a 900 MHz antenna. A 150 x 60 x 40 cm inset cube

has been graphically removed from this pseudo-image. The base of this inset cube appears to rest on bedrock surface, which provides higher amplitude (colored white and black) reflections.

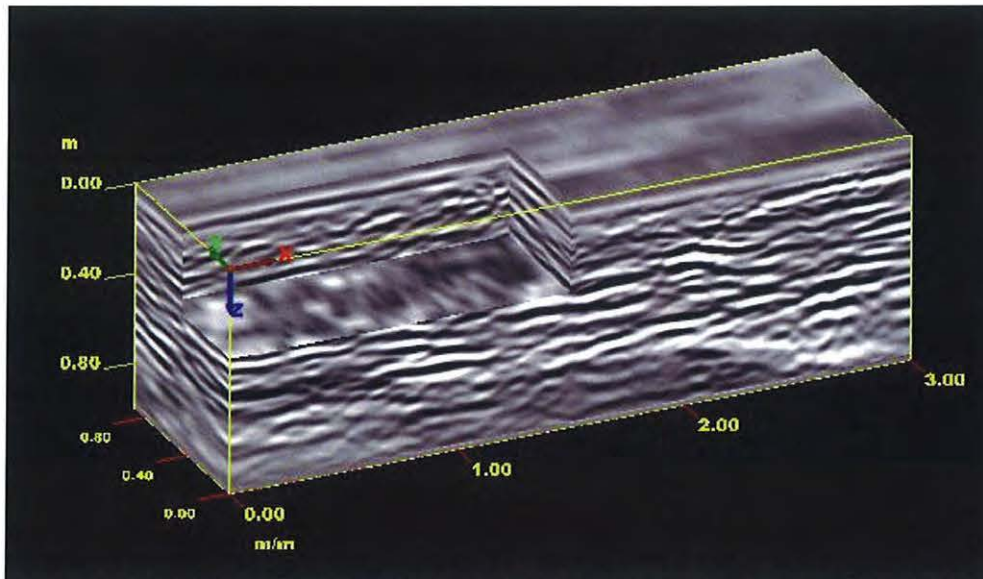


Figure 7 - This pre-wetting, 3D-pseudo-image of the Weikert grid site has a 150 by 60 by 40 cm inset cube removed. Data were collected with a 900 MHz antenna.

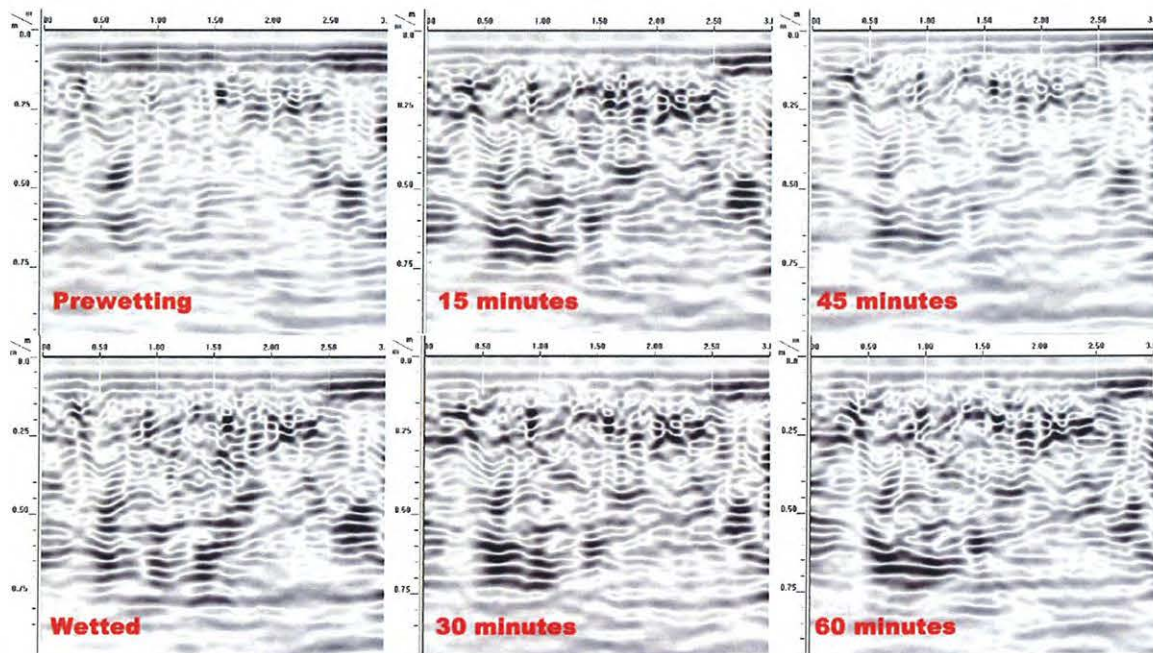


Figure 8 - Time-lapsed 2D radar records of Line 1 at the Weikert Infiltration Grid Site. All scales are in meters.

Figure 8 contains six, time-lapsed 2D radar records from Line 1 of the Weikert infiltration grid site. This line was closest to the infiltration trench and should be the first line affected by the flow of infiltrating water. With the exception of the “45-minutes” radar record, after wetting, signal amplitudes appear to increase to depths as great as 75 cm. The appearance and increased amplitudes of these reflections were

attributed to increased water contents. Some variations in reflective patterns and amplitudes on these radar records were caused by variations in the placement of the radar traverse, and antenna alignment and jarring.

On the radar records shown in Figure 8, a subsurface interface, which is believed to represent the soil/bedrock interface, spans the entire record between depths of about 45 to 55 cm. In general, after wetting, reflections from this interface appear to increase in amplitude. However, spatial variations in amplitude can be observed along this interface suggesting non-uniform distribution of soil moisture. Compare with the time lapsed 2D radar records from the Rushtown Site (see Figure 4), the similarly processed records from the Weikert Site lack hyperbolas.

In Figure 9, the radar records from Line 1 of the Weikert infiltration grid site have been transformed using a Hilbert transformation envelope. With the exception of the “45-minutes” radar record, the development of a pocket of high magnitude reflections in the central portion of this line was apparent after wetting. The development of these high magnitude reflections was attributed to increased soil moisture. In the near surface (< 25 cm), a number of high amplitude reflections appear and then vary in amplitude suggesting possible changes in dielectric permittivity associated with infiltrating water.

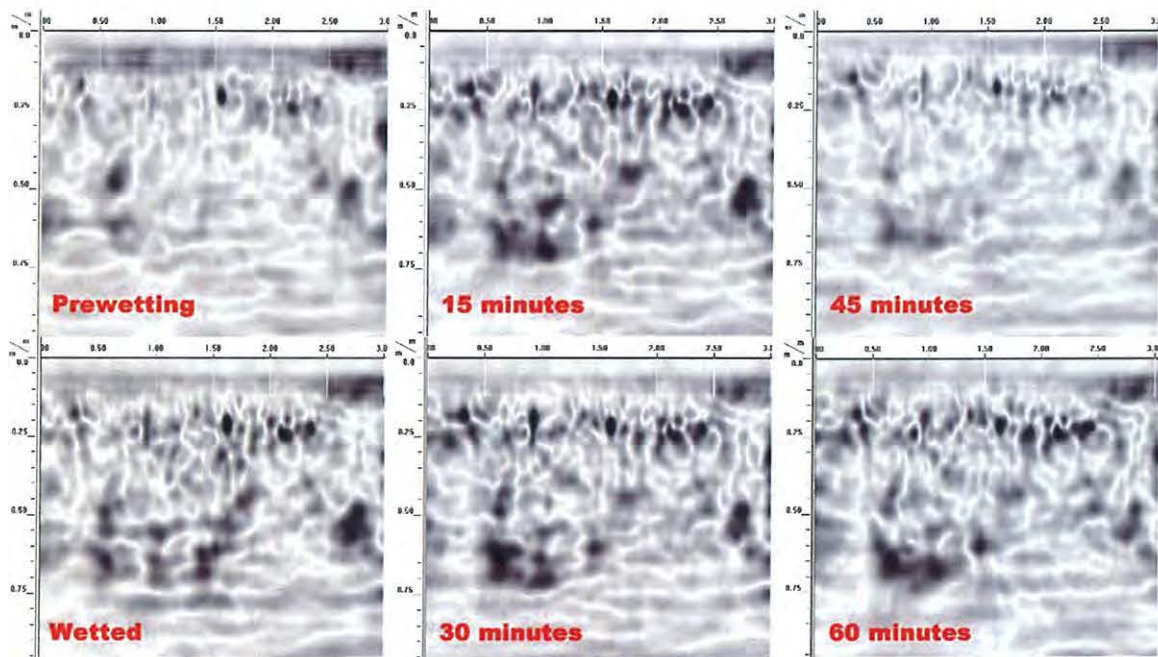


Figure 9 - Time-lapsed Hilbert Transformed 2D radar records from Line 1 at the Weikert Infiltration Grid Site. All scales are in meters.

Figure 10 contains six Hilbert transformed, time-lapsed, depth-sliced pseudo-images for both the 20 and 60 cm depth intervals. The time intervals span the duration from “pre-wetting” to 60 minutes following infiltration. The thickness of each slice was 10 cm. Subtle variations in signal amplitudes and spatial patterns were evident in these plots. However, in the depth slices shown in Figure 10, it is difficult to perceive substantial, sustained, and systematic changes in the reflective patterns that can be attributed to water flow and increased soil moisture contents. The 2D radar records shown in Figures 8 and 9 appear to provide greater information on the movement of water than the time-lapsed, time-sliced pseudo-images shown in Figure 10.

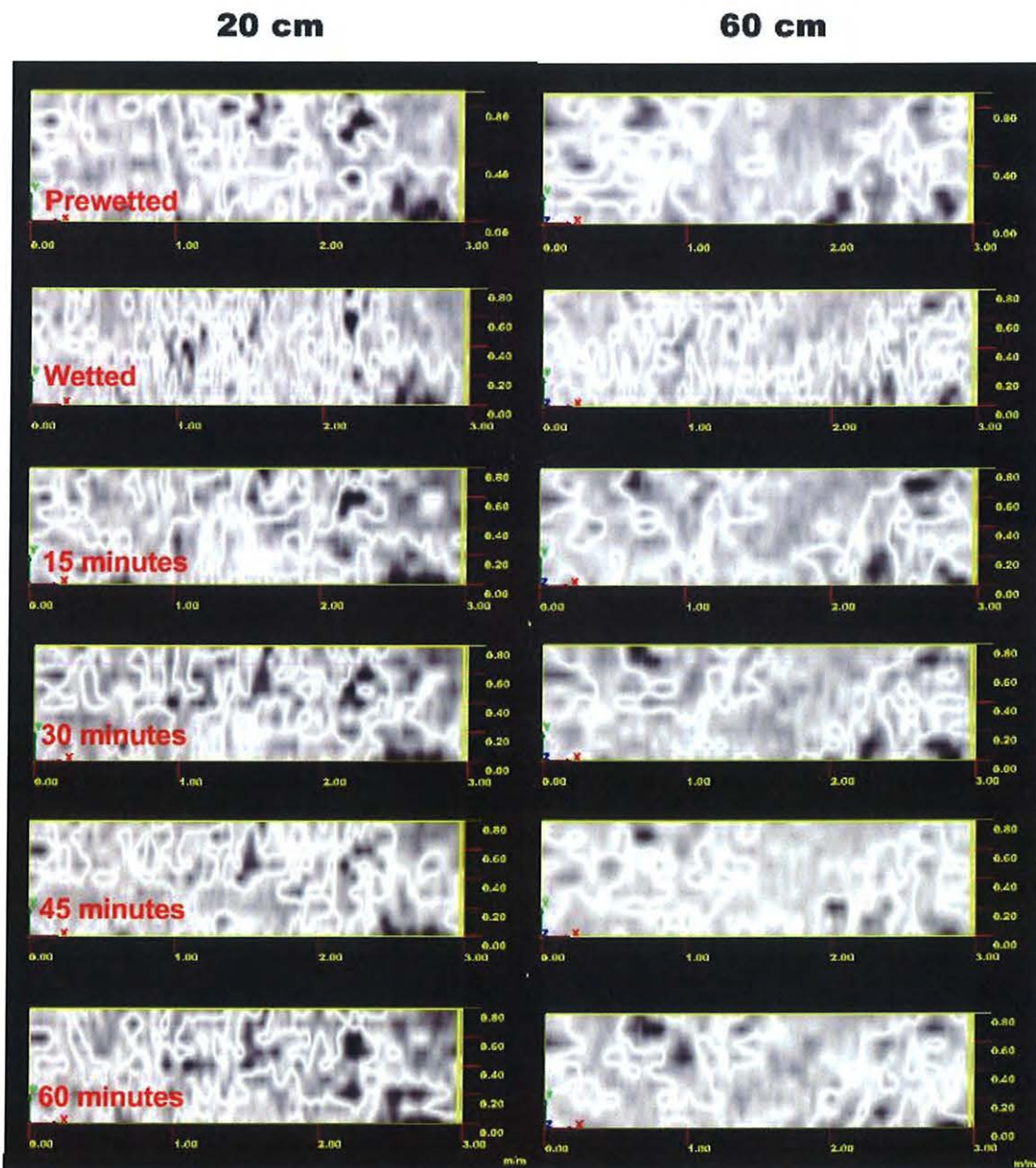


Figure 10 - These time-lapsed, depth-sliced pseudo-images from the Weikert Infiltration Site are for the 20 (left) and 60 (right) cm depth intervals. View is looking down on the grid from directly overhead.

Living Filter Field:

The sensitivity and response functions of three electromagnetic induction (EMI) sensors (Dualem-2, EM38-MK2, and Profiler) were evaluated at Pennsylvania State University's Living Filter Field. The Living Filter Research Project sprays sewage effluent onto wood land and agricultural plots as part of a wastewater renovation cycle in which the biologically active soil profile serves as the final treatment step in sewage effluent remediation. The three EMI sensors that were evaluated are used extensively by USDA, universities, and the agricultural community, and comparative surveys are needed to document their resolution, exploration depths, and response times.

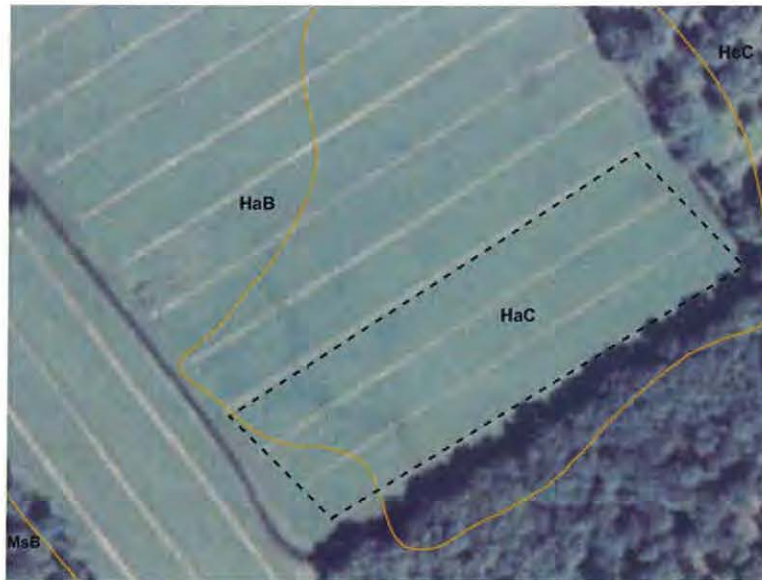


Figure 11 - This soil map contains the area that was surveyed (enclosed by segmented lines) at the Living Filter Field.

Electromagnetic induction surveys were confined to the southern portion of the Living Filter Field (see Figure 11). The area has been mapped as Hagerstown silt loam, on 3 to 8 percent slopes (HaB) and 8 to 15 percent slopes (HaC). The deep and very deep, well drained Hagerstown soils formed in residuum weathered from limestone. Hagerstown is a member of the fine, mixed, semiactive, mesic Typic Hapludalfs taxonomic family.

EMI Meters:

Three EMI sensors used in this study include: the Dualem-2 meter; EM38-MK2 meter, and the Profiler EMP-400. The depths of penetration for the Dualem-2 and EM38-MK2 meters are considered “*geometry limited*” and dependent on the instruments intercoil spacing, coil orientations, and frequency. The depth of penetration for the Profiler EMP-400 sensor is considered “*skin depth limited*” rather than “*geometry limited*.” The skin-depth represents the maximum depth of exploration, and is frequency and soil dependent: lower frequency signals travel farther through conductive mediums than higher frequency signals. The theoretical penetration depth of the Profiler EMP-400 is dependent upon the bulk conductivity of the profiled earthen material(s) and the operating frequency. For each of these EMI sensors, lateral resolution is approximately equal to the intercoil spacing. These sensors require no ground contact, are portable, and require only one person to operate.

The Dualem-2 meter is manufactured by Dualem (Milton, Ontario).³ Taylor (2000) describes the principles of operation for this meter. The Dualem-2 meter operates at a fixed frequency of 9,000 Hz and weighs about 8 kg (17.6 lbs). It consists of one transmitter and two receiver coils. One receiver coil and the transmitter coil provide a perpendicular geometry (PRP). The other receiver coil provides a horizontal co-planar geometry (HCP) with the transmitter coil. This dual-geometry array permits the simultaneous measurement of both conductivity and susceptibility over two separate exploration depths. The Dualem-2 has a 2-m intercoil spacing between the transmitter and the HCP receiver coil, and 2.1-m spacing between the transmitter coil and the perpendicular coil. This geometry provides nominal exploration depths of 1 and 3 m in the PRP and HCP geometries, respectively. The meter is calibrated at the factory and does not require field calibration. The Dualem-2 sensor comes with an internal WAAS-enabled GPS receiver, a hand-held weatherproof display/keypad/power-supply, and a carrying harness.

The EM38-MK2 meter is manufactured by Geonics Limited (Mississauga, Ontario).³ Operating procedures for the EM38-MK2 meter are described by Geonics Limited (2007). The EM38-MK2 meter operates at a frequency of 14.5 kHz and weighs approximately 5.4 kg (11.9 lbs). The meter has one transmitter coil and two receiver coils, which are separated from the transmitter coil at distances of 1.0 and 0.5 m. This dual inter-coil spacing permits the simultaneous measurement of both conductivity and susceptibility over two separate exploration depths. This configuration provides nominal exploration depths of 1.5 and 0.75 m when the meter is held in the vertical dipole orientation (VDO), and 0.75 and 0.40 m when the meter is held in the horizontal dipole orientation (HDO).

The Geonics DAS70 Data Acquisition System was used with the EM38-MK2 meter to record and store both EC_a and GPS data. The acquisition system consists of the meter, an Allegro CX field computer (Juniper Systems, Logan, Utah), and a Trimble AgGPS 114 L-band DGPS (differential GPS) antenna (Trimble, Sunnyvale, CA).³ With the acquisition system, the meter is keypad operated and measurements are automatically triggered. The RTmap38MK2 software program developed by Geomar Software Inc. (Mississauga, Ontario) was used with the EM38-MK2 meter and the Allegro CX field computer to record, store, and process EC_a and GPS data.³

The Profiler EMP-400 sensor (here after referred to as the Profiler) is manufactured by Geophysical Survey Systems, Inc. (Salem, NH).³ Operating procedures for the Profiler are described by Geophysical Survey Systems, Inc. (2008). The Profiler has a 1.22 m (4.0 ft) intercoil spacing and operates at frequencies ranging from 1 to 16 kHz. It weighs about 4.5 kg, (9.9 lbs). The Profiler is a multifrequency EMI meter that can simultaneously collect data in as many as three discrete frequencies. For each frequency, in-phase and quadrature phase data are recorded. The calibration of the Profiler is optimized for 15 kHz and, as a consequence, EC_a is most accurately measured at this frequency (Dan Delea, GSSI, personal communication). Surveys can be conducted with the sensor held in the shallower-sensing HDO or the deeper sensing VDO orientations. The sensor's electronics are controlled via Bluetooth communications with a Trimble TDS RECON-400 Personal Data Assistant (PDA).³ To collect geo-referenced data, the PDA is configured with an integral 12-channel WAAS (Wide Area Augmentation System) GPS.

To help summarize the results of the EMI surveys, the SURFER for Windows (version 10.0) software (Golden Software, Inc., Golden, CO) was used to construct the simulations shown in this report.³ The same gridding methods were used on all data.

Depth of Exploration:

As knowledge of the effective depth of exploration (d_e) is vital to interpretations, a brief discussion of this parameter is presented. McNeill (1980b) noted that a meter's d_e is geometry limited and dependent on

³ Manufacturer's names are provided for specific information; use does not constitute endorsement.

coil separation, coil orientation, and frequency. Larger coil separations and lower frequencies are used to achieve greater depths of exploration. Won et al. (1996) observed that changing the transmitter frequency will change the d_e . Won (1980 and 1983) maintains that the exploration depths of multi-frequency EMI instrument (such as the Profiler) are governed by the *skin-depth effect*: lower frequency signals travel farther through conductive mediums than higher frequency signals.

When the Dualem-2 and EM38-MK2 meters are operated under conditions of low induction number (LIN), their depth-response functions are assumed to be independent of soil conductivity. Conventionally, LIN conditions are assumed to be satisfied in soils having low (<100 mS/m) EC_a (McNeill, 1980b). However, McNeill's LIN approximations used restrictive physical and mathematical assumptions to derive a solution and are therefore considered to be valid only in more restricted physical soil settings (Callegary et al., 2007). Greenhouse et al. (1998) noted that the electrical conductivity of soils plays a critical role in the d_e obtained with all EMI sensors. Slavich (1990) and de Jong et al. (1979) reported that the d_e varies depending on the bulk electrical conductivity of the profiled material(s). Results of numerical simulations conducted by Callegary et al. (2007) indicate that the spatial sensitivity and d_e of LIN sensors varies significantly with changes in bulk electrical conductivity. Callegary et al. (2007) cautioned that only in most electrically resistive soils are the LIN approximations and its predictions of d_e correct.

With the Profiler, the depth of exploration is considered *skin depth limited* rather than *geometry limited* (Won, 1980 and 1983, Won et al., 1996). The *skin effect* is the tendency for electrical current density to be greatest at the surface and decreases exponentially with depth. *Skin depth* represents the maximum depth of exploration for the Profiler operating at a specific frequency and sounding a medium of known conductivity. Theoretically, the maximum d_e or *skin depth* is inversely proportional to frequency (Won et al., 1996). Low frequency signals have longer periods of oscillation, loose energy less rapidly, and supposedly achieve greater depths of exploration than high frequency signals. In addition, for a given frequency, the d_e is greater in low than in high conductivity soils.

Brosten et al. (2011) noted how multifrequency EMI sensors continue to challenge users. Brosten et al. (2011), using synthetic modeling methods, determined that a GEM-2 multifrequency sensor (similar to the Profiler), in a medium with an estimated skin depth of 23.4 m (76.8 ft), had an actual depth of exploration that ranged from only 1.8 to 2.7 m (5.9 to 8.9 ft). Based on the findings of Brosten et al. (2011), the Profiler is viewed by this observer as a *geometry limited* sensor, like the Dualem-2 and EM38-MK2 meters. Assuming LIN conditions, the effective exploration depths of the Profiler (when placed on the ground surface) is assumed to be approximately 1.8 m (5.9 ft) and 0.92 m (3.0 ft) in the VDO and HDO, respectively. However, as a result of the aforementioned studies by Callegary et al., (2007) the manufacturer's specified effective exploration depths for these EMI sensors are considered greater than the actual depths of observation.

Field Procedures:

At a designated calibration point, the EM38-MK2 meter and the Profiler were calibrated to the existing soil conditions. The Dualem-2 meter requires no field calibration. Each EMI sensor was operated in the VDO and in the continuous recording mode. Each sensor was towed on sleds behind a 4WD all-terrain-vehicle. The operating height above the ground varied with each sensor. The Dualem-2 and EM38-MK2 meters were operated at a height of about 6 and 4 cm, respectively. The Profiler was placed on top of a sled at a height of about 28 cm above the ground surface. The number of measurement per second did vary with the sensor (Dualem-2 meter and Profiler, one measurement every 2 seconds; EM38-MK2, two measurement per sec). The locations and number of traverse lines were similar for each EMI sensor. The data were not temperature corrected.

Results:

Basic statistics for the EC_a data collected with the three EMI sensors at the Living Filter Field are listed in Table 1. Data collected with the three sensors are considered similar. Negative values are attributed to metallic artifacts scattered or buried across the study site. The averaged values for shallower-sensing PRP (DuaLEM-2) and HDO (EM38-MK2) were 22.4 and 23.1 mS/m, respectively. In the deeper-sensing HCP (DuaLEM-2), slightly lower and more variable EC_a measurements were recorded than in the VDO of the Profiler and EM38-MK2. Slightly higher and less variable EC_a were recorded with the EM38-MK2 meter. These small variations reflect differences in the depth of exploration and volume of soil material measured with each sensor, operating frequency, sensor calibration, number of recorded measurements, and soil's conductivity profile.

As effluent is being sprayed on the field, higher EC_a values were anticipated for the surface layers. However, this relationship was not manifested in the data collected at this site. The solum thickness of Hagerstown soil ranges from 1.0 to 1.82 m (40 to 72 inches). The subsoil (at a depth of 15 to 50 cm (6 to 20 inches)) produces a noticeable clay bulge with a weighted, average clay content between 35 and 60 percent. The higher clay content of the subsoil may partially explain the higher averaged EC_a measured with the 100 cm intercoil spacing of the EM38-MK2 meter and the Profiler. In the lower part of the subsoil, the clay content decreases by more than 20 percent if the soil is deeper than 1.52 m (60 inches). Depth to hard, more electrically resistive limestone ranges from 1 to 2.1 m (40 to 84 inches) or more. The lower clay content and the possible presence of limestone at lower soil depths helps to explain the lower averaged EC_a recorded with the DuaLEM-2 meter operated in the deeper-sensing HCP.

Table 1. Basic Statistic for the apparent conductivity data collected with the three EMI sensors at the Living Filter Field.

	Profiler 15000 Hz	EM38-MK2 100 -cm	EM38-MK2 50-cm	DuaLEM-2 HCP	DuaLEM-2 PRP
Number	1289	2469	2469	1266	1266
Minimum	14.8	-3.8	-75.4	-36.4	7.8
25%-tile	20.2	25.1	21.4	18.5	20.2
75%-tile	26.5	28.8	24.6	23.6	23.8
Maximum	44.2	45.9	36.3	66.6	105.8
Mean	23.6	27.1	23.1	21.4	22.4
Std. Dev.	4.2	3.0	3.5	5.0	5.8

In a theoretical discussion on EMI, McNeill (1980a) observed that the measured EC_a is a function of the instruments' calibration, coil separation, coil orientation, and frequency. McNeill (1980a) also observed that EC_a values are seldom diagnostic in themselves. However, spatial patterns and the relative magnitudes of EC_a do provide inferential clues as to differences in soils and soil properties.

Figures 12, 13, and 14 show spatial EC_a patterns derived from data collected with the DuaLEM-2, EM38-MK2 and Profiler, respectively. In each plot, the same color ramp, scale and interval has been used to aid comparison. The magnitudes of the EC_a measurements obtained within the study site are believed to principally reflect differences in soil moisture and clay contents and the presence of buried artifacts. With minor exceptions and regardless of device, dipole geometry, frequency or exploration depth, the spatial patterns shown in Figures 12, 13, and 14 for similar dipole orientations and geometries appear remarkably similar.

Though best displayed in the data collected with the DuaLEM-2 meter and the Profiler, EC_a measurements were strongly affected by a buried conductor, which partially crosses the lower-center portion of the plots. This feature was later confirmed to be a pipe that was buried at a depth of about 1.22 m (4 ft) below the surface. In addition, two other lateral pipes are suggested in the data collected in the deeper-sensing plots simulated from the EC_a data collected with the DuaLEM-2 (operated in the HCP), the EM38-MK2

(measured with the 100-cm intercoil spacing), and the Profiler. These two lateral pipes appear to extend in a northeast direction away from the known buried pipe. It can be notice that the Profiler provided better positioning of the known pipe, whereas there appears alternating lag or an offset over the pipe in both the Dualem-2 and EM38-MK2 plots (Figures 12 and 13). Because of the distance between the transmitting and receiving coils and the time delay in data logging, slight spatial discrepancies exist in EMI data collected with the Dualem-2 and EM38-MK2 sensors. These offsets and delays, as well as the gridding methods and contour intervals used in computer simulations, are responsible for the alternating lag or offset that can be observed in the spatial data collected with these sensors.

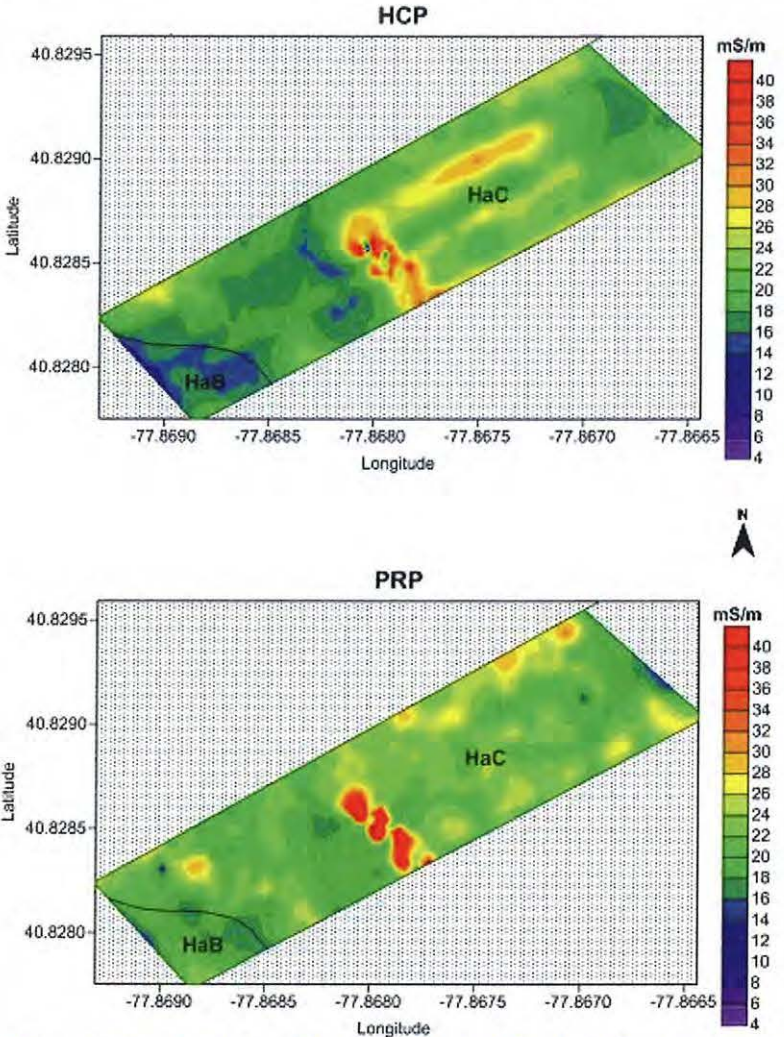


Figure 12 - Spatial EC_a patterns for data collected with the Dualem-2 meter operated in the deeper-sensing HCP (upper plot) and the shallower-sensing PRP (lower plot).

With the exception of the responses from the buried artifacts, spatial EC_a patterns are believed to principally reflect differences in soil moisture and clay contents, and soil architecture. Excluding data from the buried pipes, EC_a appears to increase with depth for the EM38-MK2 meter (measurements in the VDO greater than those in the HDO) and decrease with depth for the Dualem-2 meter (measurements in the PRP greater than those in the HCP). This difference can be associated with differences in the exploration depths of these meters when operated in different dipole geometries, and soil architecture (presence of clay bulge and limestone bedrock).

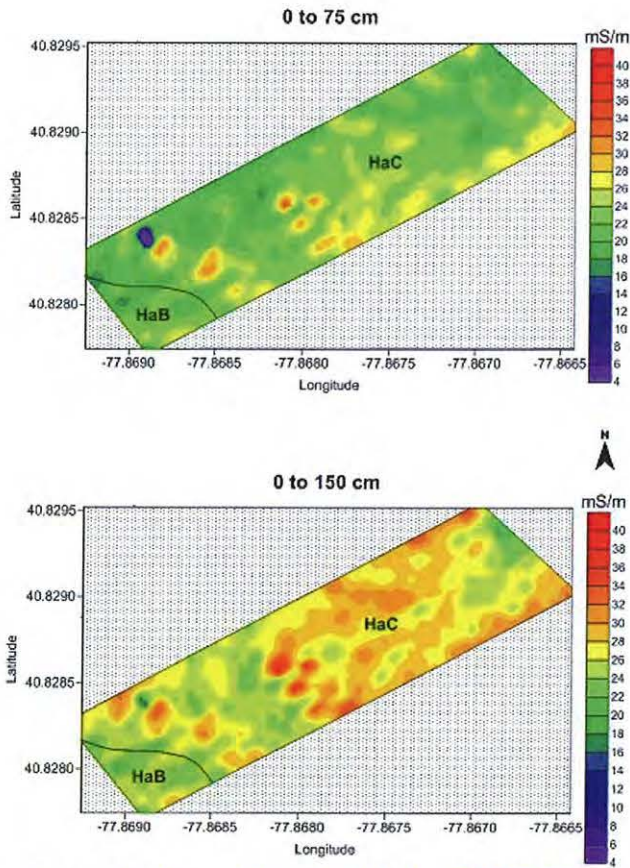


Figure 13 - Spatial EC_a patterns for data collected with the EM38-MK2 meter and measured with the shallower-sensing 50-cm (upper plot) and deeper-sensing 100-cm (lower plot) intercoil spacings.

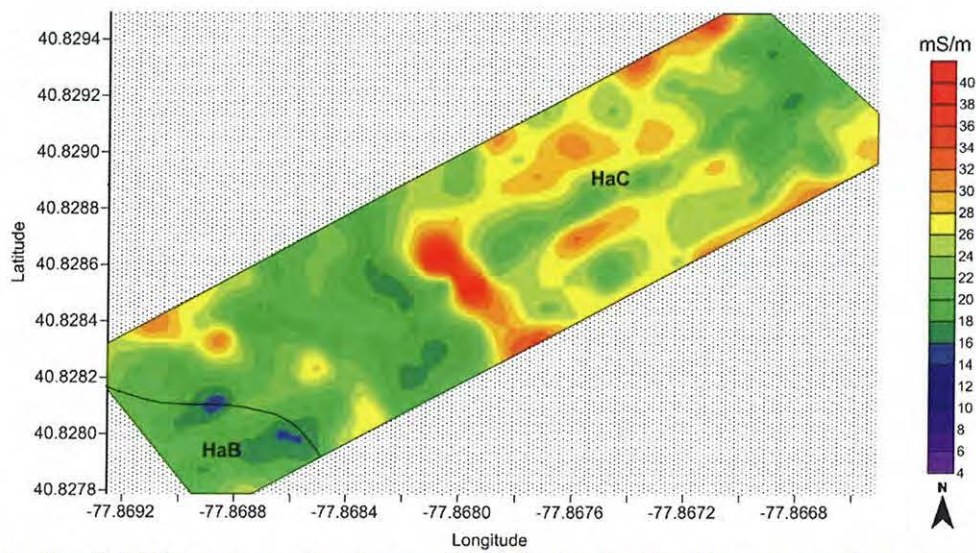


Figure 14 - Spatial EC_a patterns for data collected with the Profiler operated at a frequency of 15000 Hz.

The pipe represents a straight, narrow conductor. The zigzag pattern over the pipe, which is evident in the data collected with the Dualem-2 and EM38-MK2 sensors, is incorrect. It is assumed that the data from these two meters were recorded at different times than the recorded GPS position. Differences in the approximate synchronization between the EMI sensors and the GPS receiver, and the response integration time of the sensors are responsible for these zigzag patterns. Manual position corrections were applied to the data collected with these two meters, and revised plots developed. In Figures 15 and 16, the Dualem-2 and the EM38-MK2 meter data have been manually repositioned in order to account for the offset caused by traversing the survey area in two different directions (back and forth across the field). Repositioning was not required for the Profiler data.

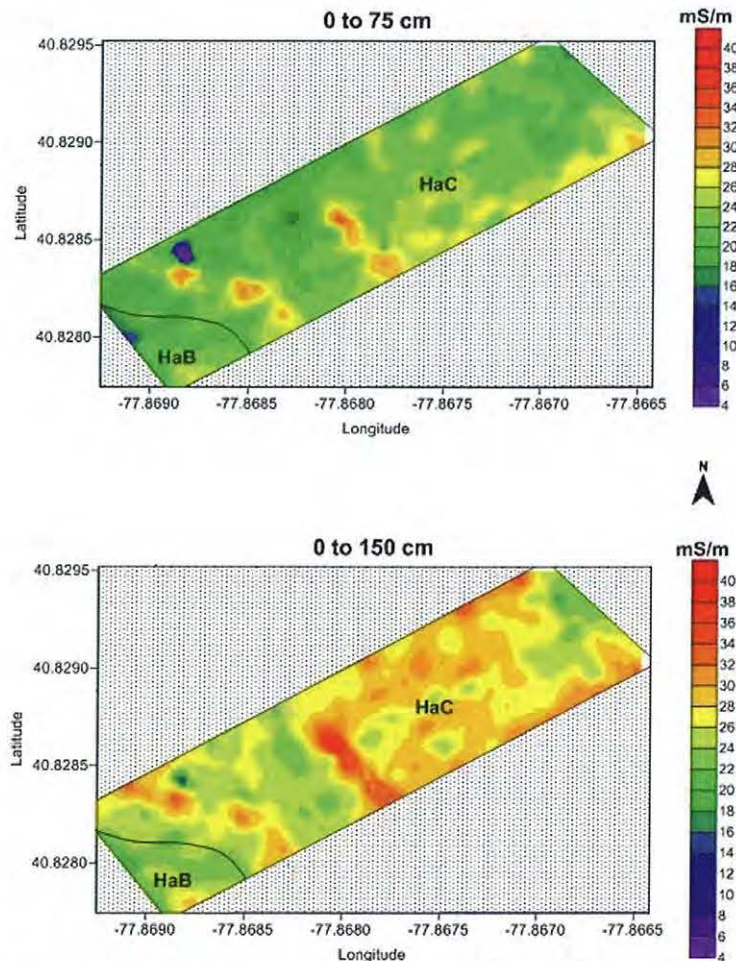


Figure 15 - Revised plots of the data collected with the EM38-MK2 meter with the positional data manually adjusted.

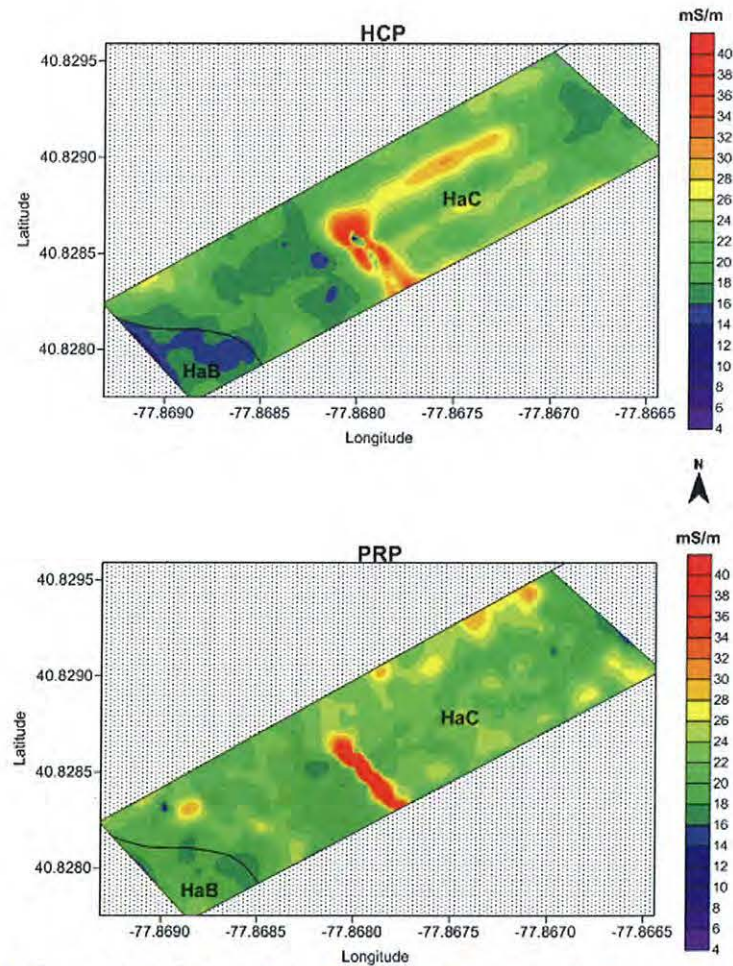


Figure 16 - Revised plots of the data collected with the Dualem-2 meter with the positional data manually adjusted.

References:

Brosten, T.R., F.D. Day-Lewis, G.M. Schultz, G.P. Curtis, and J.W. Lane, 2011. Inversion of multi-frequency electromagnetic induction data for 3D characterization of hydraulic conductivity. *Journal of Applied Geophysics* 73: 323-335.

Callegary, J.B., T.P.A Ferré, and R.W. Groom, 2007. Vertical spatial sensitivity and exploration depth of low-induction-number electromagnetic-induction instruments. *Vadose Zone Journal* 6: 158-167.

Daniels, D. J., 2004. *Ground Penetrating Radar*; 2nd Edition. The Institute of Electrical Engineers, London, United Kingdom.

de Jong, E., A.K. Ballantyne, D.R. Cameron, and D.L. Read, 1979. Measurement of apparent electrical conductivity of soils by an electromagnetic induction probe to aid salinity surveys. *Soil Sci. Soc. Am. J.* 43:810-812.

Geonics Limited, 2007. EM38-MK2 ground conductivity meter operating manual. Geonics Ltd., Mississauga, Ontario.

- Geophysical Survey Systems, Inc., 2008. Profiler EMP-400 User's Manual. Geophysical Survey Systems, Inc., Salem, New Hampshire.
- Greenhouse, J.P., D.D. Slaine, and P. Gudjurgis, 1998. Application of geophysics in environmental investigations. Matrix Multimedia, Canada. CD-ROM.
- Jol, H., 2008. Ground Penetrating Radar: Theory and Applications. Elsevier Science, Amsterdam, The Netherlands.
- McNeill, J.D., 1980a. Electrical Conductivity of soils and rocks. Technical Note TN-5. Geonics Ltd., Mississauga, Ontario.
- McNeill, J.D., 1980b. Electromagnetic terrain conductivity measurement at low induction numbers. Technical Note TN-6. Geonics Limited, Mississauga, Ontario.
- Rhoades, J.D., P.A. Raats, and R.J. Prather, 1976. Effects of liquid-phase electrical conductivity, water content, and surface conductivity on bulk soil electrical conductivity. *Soil Sci. Soc. Am. J.* 40:651-655.
- Slavich, P.G., 1990. Determining EC_a-depth profiles from electromagnetic induction measurements. *Aust. J. Soil Res.* 28:443-452.
- Taylor, R. S. 2000. Development and applications of geometric-sounding electromagnetic systems. Dualem Inc., Milton Ontario.
- Won, I.J., 1980. A wideband electromagnetic exploration method - Some theoretical and experimental results. *Geophysics* 45:928-940
- Won, I.J., 1983. A sweep-frequency electromagnetic exploration method. pp. 39-64. IN: A.A. Fitch (editor) Development of Geophysical Exploration Methods. Elsevier Applied Science Publishers, Ltd. London.
- Won, I.J., D.A. Keiswetter, G.R.A. Fields, and L.C. Sutton, 1996. GEM-2: A new multifrequency electromagnetic sensor. *Journal of Environmental & Engineering Geophysics* 1:129-137.

Appendix 1: GPR File Numbers associated with different radar traverses and study sites.

File #	Purpose	Antenna	Location
1	Buried Plate at 50 cm; 60 ns	400 MHz	Permanent Grid
2-13	Permanent Grid	400 MHz	Permanent Grid
15 to 21	Dry Run	400 MHz	Rushtown Site
22 to 29	Dry Run	900 MHz	Rushtown Site
	Added 7 gallons water		
37 to 44	+ 5 minutes	900 MHz	Rushtown Site
45 to 52	+ 15 minutes	900 MHz	Rushtown Site
53 to 60	+ 30 minutes	900 MHz	Rushtown Site
61 to 68	+ 45 minutes	900 MHz	Rushtown Site
69 to 77	+ 60 minutes	900 MHz	Rushtown Site
77 to 84	+ 120 minutes	900 MHz	Rushtown Site
85 to 92	+ 130 minutes	400 MHz	Rushtown Site
	Additional 7 gallons		Rushtown Site
93 to 100	11:55	400 MHz	Rushtown Site
101 to 108	12:05	900 MHz	Rushtown Site
	Weikert Site		
109	Buried Plate at 50 cm	900 MHz	Weikert Site
111 to 119	Dry Run	900 MHz	Weikert Site
120 to 128	Dry Run	400 MHz	Weikert Site
129	Jarring Antenna Run	900 MHz	Weikert Site
	Added 7 gallons water		
130 to 138	+ 5 minutes	900 MHz	Weikert Site
139 to 147	+ 15 minutes	900 MHz	Weikert Site
148 to 156	+ 30 minutes	900 MHz	Weikert Site
157 to 165	+ 45 minutes	900 MHz	Weikert Site
166 to 174	+ 60 minutes	900 MHz	Weikert Site
	Additional 14 gallons		Weikert Site
175 to 183	+ 5 minutes	900 MHz	Weikert Site
184 to 192	+ 10 minutes	400 MHz	Weikert Site